Acta Oceanol. Sin., 2019, Vol. 38, No. 1, P. 22–31
https://doi.org/10.1007/s13131-019-1367-9
http://www.hyxb.org.cn
E-mail: hyxbe@263.net

Temperature variability caused by internal tides in the coastal waters of east coast of Peninsular Malaysia

Nur Hidayah Roseli[1], Mohd Fadzil Akhir[1]*

[1] Institute of Oceanography and Environment, Universiti Malaysia Terengganu, Terengganu 21030, Malaysia

Received 25 October 2017; accepted 6 February 2018

Abstract

The effects of tidal currents (i.e., barotropic and internal tides) are important in the biogeochemistry of a coastal shelf sea. The high-frequency of currents and near-bottom temperatures collected in three consecutive southwest monsoon seasons (May, June, July and August of 2013 until 2015) is presented to reveal the role of the tidal currents to the temperature variability in the coastal shelf sea of the east coast of Peninsular Malaysia (ECPM), south of the South China Sea (SCS). The results of a spectral density and harmonic analysis demonstrate that the near-bottom temperature variability and the tidal currents are influenced by diurnal (O_1 and K_1) and semidiurnal (M_2) tidal currents. The spectral density of residual currents (detided data) at 5, 10 and 16 m depth also shows significant peaks at the diurnal tidal frequency (K_1) and small peaks at the semidiurnal tidal frequency (M_2) indicating the existence of internal tides. The result of the horizontal kinetic energy (HKE) shows a strong intermittent energy of internal tides in the ECPM with the strongest energy is found at 16 m depth during a sporadic cooling event in June and July. A high horizontal cross-shore heat flux (16 m) also indicates strong intrusions of cooler water into the ECPM in June and July. During the short duration of cold pulse water observed in June and July, a cross-wavelet analysis also reveals the strong relationship between the near-bottom temperatures and the internal tidal currents at the diurnal tidal frequency. The intrusion of this cooler water is probably related to the monsoon-induced upwelling in June. It is loosely interpreted that the interaction between the strong barotropic tides and the steep slope in the central basin of the SCS under the stratified condition in southwest monsoon has generated these internal tides. The dissipation of internal tides from the slope area probably has driven the cold-upwelled water into the ECPM coastal shelf sea when the upwelling intensity is the highest in June and July.

Key words: east coast of Peninsular Malaysia, South China Sea, barotropic tidal currents, internal tides, near-bottom temperature, coastal shelf sea

Citation: Roseli Nur Hidayah, Akhir Mohd Fadzil. 2019. Temperature variability caused by internal tides in the coastal waters of east coast of Peninsular Malaysia. Acta Oceanologica Sinica, 38(1): 22–31, doi: 10.1007/s13131-019-1367-9

1 Introduction

The east coast of Peninsular Malaysia (ECPM) is located in the southern region of the South China Sea (SCS). The region with a tropical climate like the southern SCS received greater heat from the sun and experienced high precipitation throughout the years (Wyrtki, 1961). In order to provide a basis for the sustainable management of the coastal shelf seas like the ECPM, many multidisciplinary studies had been done along the ECPM since the work of Wyrtki (1961). Unfortunately, the physical-oceanography-related-studies in the ECPM are lacking especially in the interaction between tidal dynamics and temperature variability at scales shorter than a seasonal scale.

In this region, the sea temperatures varied seasonally due to the monsoonal effects, northeast monsoon (November–March) and southwest monsoon (June–September) (Akhir et al., 2011; Akhir, 2012; Wyrtki, 1961); with the southwest monsoon recorded a warmer sea surface temperature than the northeast monsoon. Despite much warmer temperature recorded near the surface, the cooler water was recently observed on the near-bottom of the ECPM coastal shelf sea in June (Roseli et al., 2015). This cooler water was probably brought into the ECPM by a monsoon-induced-upwelling that occurred during the southwest monsoon (Akhir et al., 2015; Dippner et al., 2007).

Similar to the most coastal shelf seas around the world, tides of the adjacent basin play the major role in the dominant motion of the ECPM's coastal system (Robinson, 1983). The tidal currents in the ocean can be separated into the barotropic and baroclinic tides. The concept of barotropic and baroclinic was implemented to understand the internal tides in the ocean (Torgrimson and Hickey, 1979). Most of the literatures regarding tides in the southern SCS (0°–7°N, 100°–120°E) are based on a satellite altimetry and model simulated outputs. The analysis of tides using satellite altimetry data by Yanagi et al. (1997) and Zu et al. (2008) did mention that the diurnal tides dominated the whole SCS region. The model simulation by Tangang et al. (2011) and Daryabor et al. (2016) also verified the predominant diurnal of K_1 tidal harmonic constituent near the ECPM. At the same time the semidiurnal M_2 also predominantly dominated the ECPM region.

Foundation item: The Higher Institutional Centre of Excellent Universiti Malaysia Terengganu under contract No. TJ66928; the Malaysia Coastal Observation Network Project under the Institute of Oceanography and Environment, Universiti Malaysia Terengganu of Malaysia.
*Corresponding author, E-mail: mfadzil@umt.edu.my

Although many kinds of literature had confirmed the predominant diurnal K_1 and semidiurnal M_2 in the ECPM region, the existence of the internal tides in the ECPM (baroclinic tides) has never been mentioned in any kinds of literature before.

The internal tides are the internal waves that propagate at the tidal frequencies and generated when the barotropic tides flow over the varying bottom topography under the stratified condition (Mihanović et al., 2006; Smith et al., 2016; Subeesh and Unnikrishnan, 2016; Wu et al., 2013). In other regions, many studies had revealed the significant relationship among the internal tides and temperature variability using the high frequency moored currents and temperature datasets (i.e., Bravo et al., 2013; Kaplan et al., 2003; Mihanović et al., 2009; Pidgeon and Winant, 2005). Studies that related the sea temperatures variability and relative forcing mechanism in the SCS focused more on the interannual and seasonal time scales (Akhir et al., 2011; Chern and Wang, 1994; Chu et al., 1999; Roseli et al., 2015; Saadon and Camerlengo, 1996) where the seasonal temperatures variations in the southern SCS were small and never exceed 2°C (Huang et al., 1997). There is one study that reported daily mean temperatures, velocities and tide levels in the ECPM (Taira et al., 1996) but did not mention any role of the internal tides to the daily temperature variability.

Under the Malaysia Coastal Observation Network Project, this study aims at improving knowledge of the processes involved in the coastal shelf sea off the ECPM. To address the way the physical processes interact with each other in a higher temporal time scale, we used the results of high-frequency water level, current velocities and near-bottom temperatures to investigate the role of barotropic and internal tidal currents in the near-bottom temperatures variability. The paper will first describe the near-bottom temperature and barotropic tidal currents characteristics in the ECPM area. It is important to first provide basic knowledge regarding a barotropic condition to understand the internal tidal feature in an area. It is because the baroclinic (internal tides) energy is generated from the interaction between the barotropic tidal energy and the bottom topography. We will then determine the influence of the barotropic and internal tides on the near-bottom temperature fluctuations which then lead to the understanding of temporal variability in the sea temperatures off the ECPM. This is the first time the internal tides feature will be presented and discussed in the ECPM region.

2 Materials and methods

2.1 *Data sources*

The main datasets used in this present study came from mooring data deployed in the coastal region of ECPM (5°26.571′N, 103°9.636′E), with a depth of less than 20 m: Station A (Fig. 1). Measurements of current velocities, pressure, and near-bottom temperatures were collected using Acoustic Wave and Current Profiler (AWAC) deployed at the coastal area of ECPM recording at 5 min intervals. Observations at Station A were carried out during the southwest monsoon season from May to August (MJJA) in 2013 to 2015 (Table 1).

Although the research provided the high-frequency and long observed data, we are aware of the limitation of the study. The research was conducted based on observed data from one location, which is very near to the coast (<20 m). The observations at several other points towards the shelf edge (i.e., middle shelf and shelf edge) would provide consistent internal tidal signals if available. Unfortunately, we lose our mooring equipment deployed at the middle shelf area (~50 m) and it is difficult for us to retrieve it back. Besides, it is impossible for us to deploy any mooring equipment at the shelf edge because the area is beyond the Malaysia's Exclusive Economic Zone (EEZ). Thus, the entire analysis done in this study is based on the observed data collected in only one location (near the coast with depth less than 20 m).

2.2 *Data processing and analysis*

The total depth of the mooring station is approximately 20 m. The water level data was obtained by subtracting the depth 20 m from the AWAC depth data. The data of depth was converted from pressure data using TEOS–10 (http://www.TEOS–10.org). The temperature is recorded using the thermistor that embedded in the AWAC's head. The temperature data were collected at 16 m depth, two to three meters above the bottom.

The AWAC collected the current speed and direction in one meter thick layers from the bottom to the surface. The current speeds and directions were first converted into velocity compon-

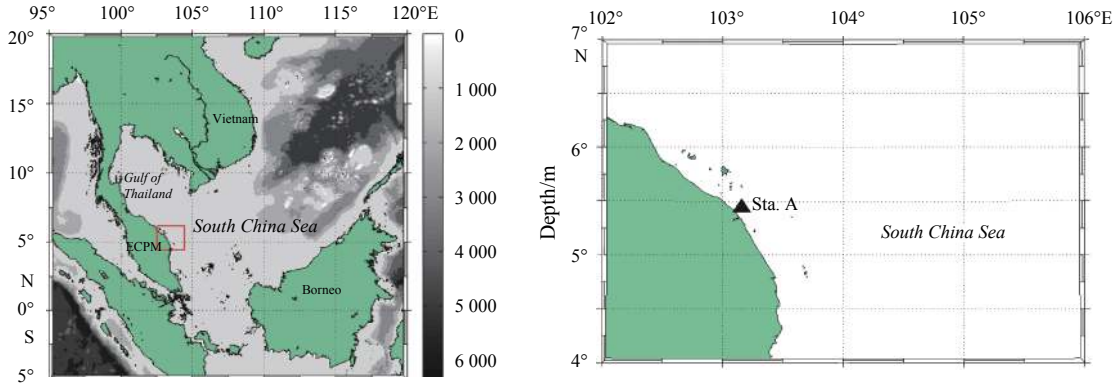

Fig. 1. Location of mooring site (Station A) in the ECPM coastal sea.

Table 1. Details of AWAC profiler's and thermistors' deployment

Station	Day/Month/Year	Instruments deployed	Depth/m	Level(bin size)/m
A	1/5/2013–31/8/2013	AWAC	20	3–16(1)
5°26.571′N, 103°9.636′E	25/5/2014–28/8/2014	AWAC	20	3–16(1)
	1/5/2015–31/8/2015	AWAC	20	3–16(1)

ents (u and v). Current velocities data were then rotated into a common coordinate system using the angle of the principal axis of currents, 40° relatives to the north, which is roughly aligned with the direction of the coast at ECPM. After the rotation, the u-component was now positive for northeastward across the ECPM coastline and the v-component was positive for northwestward along the ECPM coastline. The rotated current velocities were averaged vertically, with the two deepest layer and two surface layer being excluded since they are influenced by bottom friction and AWACs' poor measurements (Mihanović et al., 2009).

The harmonic analysis was performed on the depth-averaged currents, using the *T_Tide* Matlab package (Pawlowicz et al., 2002). The residual currents were obtained by subtracting the barotropic tidal signal from the total currents at 5, 10 and 16 m depth. The existence of internal tides feature was determined from these residual currents. Spectral analysis was performed on the residual currents data. If the influence of tides was significant in the spectral density plot, the internal tides were said to exist in the currents data. The similar toolbox also was used to calculate the amplitude, phase, and inclination of tidal constituents in the barotropic tidal currents in order to determine the ellipse parameters.

In addition, the horizontal kinetic energy (HKE) was calculated to compare the energy of barotropic currents and residual currents (5, 10 and 16 m) to verify that the internal tides are not negligible in this study. The HKE was defined as $\rho(u^2+v^2)/2$, where ρ is seawater density (here estimated as 1 025 kg/m^3), u is u-velocity component and v is v-velocity component (Ma et al., 2013; Zhang et al., 2014).

To understand the coastal dynamic processes related tidal flow and near-bottom temperature variability in the coastal shelf sea area, the wavelet analysis method was used (Grinsted et al., 2004; Ng and Chan, 2012a, b). The wavelet transform was used to analyze the power contained in the series at different frequencies while cross-wavelet transform was used to compare two-time series by identifying their common power (Mihanović et al., 2006). The wavelet spectra at diurnal scale (20 to 28 h) from the results of both the wavelet transform and the cross-wavelet transform are extracted and discussed. The two-series are first normalized by the respective variances. We used 95% confidence level to determine coherence as significant. Two series are said to have a significant relationship if the spectra show consistent or slowly changing phase angles (minimum phase angle shift) (Ng and Chan, 2012b).

Horizontal heat flux was calculated based on the equation of $F = \rho C_p T' V'$, where ρ is seawater density (here estimated as 1 025 kg/m^3), C_p is the specific heat (3 993 J/(kg·°C)), T' is the near-bottom temperature (°C) and V' is the near-bottom cross-shore velocity vector (Smith et al., 2016).

3 Results

3.1 *Near-bottom temperature variability*

Temperatures in the tropical coastal region depend both on seasonal and daily variations. The near-bottom (refer to 16 m depth in this study) temperatures taken during the southwest monsoon, MJJA months are presented in Fig. 2. Overall, the near-bottom temperatures in the coastal of ECPM during these particular seasons varied monthly and daily. During these years, the warmest near-bottom (16 m) temperatures of the ECPM were recorded in May. The temperatures suddenly decreased in June and fluctuated within a lower range of temperatures (25 to 26.5°C) until July.

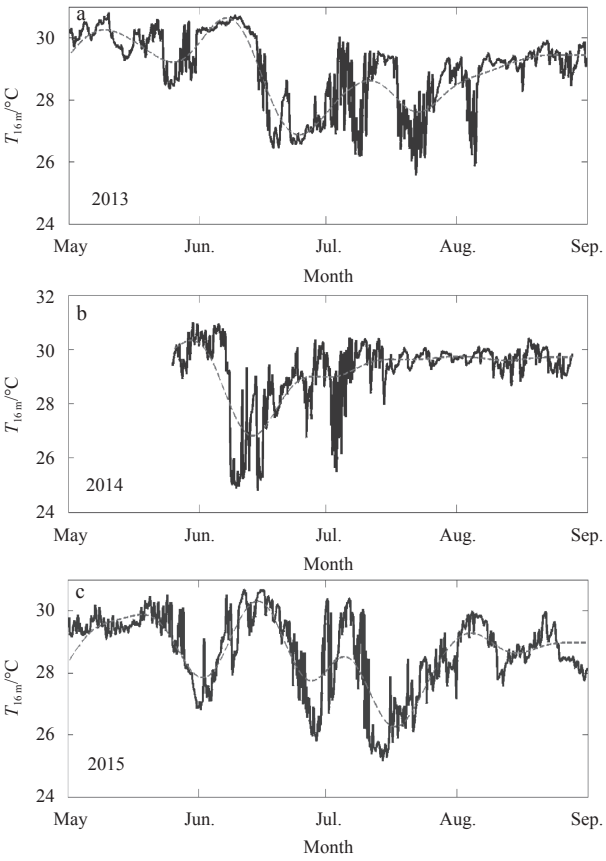

Fig. 2. Time series of near-bottom temperatures (16 m) collected in MJJA months of 2013, 2014 and 2015.

The significant drop in temperature is unusual for tropical waters, such as the southern SCS, and had never been recorded previously in the region. There were times when the temperature values increased up to 30°C, but after a few days, the temperature decreased. In 2013, this episodic event occurred until early August, but in 2014 and 2015, it ended in the middle of July and at the end of July, respectively. The monthly average of horizontal

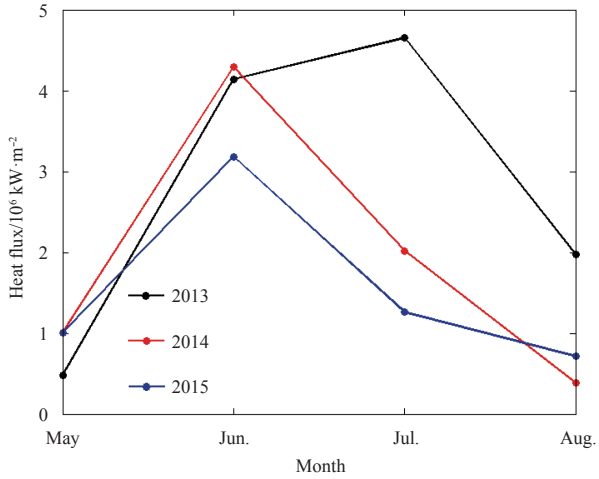

Fig. 3. The monthly average of horizontal near-bottom heat flux calculated from near-bottom temperature and near-bottom cross-shore velocities vector in MJJA months of 2013, 2014 and 2015.

near-bottom heat flux presented in Fig. 3 also shows the highest value in June. In 2013, the heat flux is increasing until July. However, the horizontal near-bottom heat flux is decreasing in 2014 and 2015. The horizontal near-bottom heat flux was then decreased in August for all three years.

The power spectral densities (PSD) of near-bottom temperatures presented in Fig. 4 revealed the daily fluctuations in the temperatures variability. Although the variance of lower frequency (>24 h) spectra is greater than both 24 and 12 h frequencies (not shown), the narrowest peak is achieved in the 24 h frequency band.

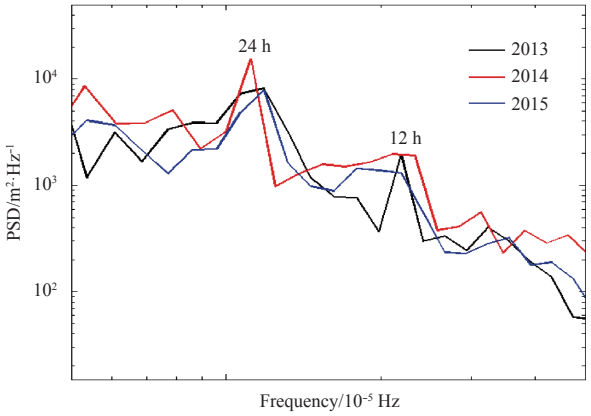

Fig. 4. Spectral density plot of near-bottom temperatures (16 m) taken in MJJA months of 2013, 2014 and 2015. The power spectral density is calculated based on 95% significance interval (not shown here).

3.2 *Tidal currents*

Information on tidal currents in this study was obtained from the high frequency of currents data recorded at the simultaneous time as near-bottom temperatures (16 m). Although the spatial distribution is limited, the data do give considerable insight as to how the tidal parameters vary in the region.

In this paper, the diurnal band, which frequencies close to 24 h period, includes the gravitational tidal constituents of O_1 and K_1. The semidiurnal band, which frequencies close to 12 h period, includes the gravitational constituents of M_2 and; the constituent based on solar radiation, S_2. Tidal ellipse parameters obtained from the harmonic analysis (Pawlowicz et al., 2002) was used to investigate the tidal fluctuations contained in the barotropic tidal currents (Table 2). The highest amplitude for the barotropic currents for three consecutive southwest monsoon seasons in the ECPM is the diurnal tide. The highest amplitude for the barotropic tidal harmonic is the diurnal K_1 (0.13 m/s). The second highest is the O_1 amplitude with 0.12 m/s. The barotropic tidal currents amplitudes for the semidiurnal constituent were observed in the M_2 constituents (0.07 m/s). The semidiurnal constituent of S_2 was comparatively small with amplitudes of 0.012 m/s.

The tidal ellipse of major tidal constituents of barotropic currents was plotted and presented in Fig. 5. The tidal ellipse is specified by the major and minor axes being the maximum and minimum tidal current velocities along with the inclination of the ellipse and the phase. The strongest tidal current velocities were observed in the diurnal O_1 and K_1; and semidiurnal M_2 tidal band constituents. The diurnal ellipses of the K_1 tidal harmonic constituent were oriented perpendicular to the coast, with the major axis amplitudes being less than 0.13 m/s. The angles perpendicular to the coast indicates a dominant cross-shore flow and the tip of the ellipse verified the onshore direction of the tidal currents. The M_2 direction also differed with the O_1 and K_1 tidal ellipses where the M_2 ellipse tip was pointing away from the shore. The diurnal ellipses (O_1 and K_1) are rotated counterclockwise from the east while the semidiurnal ellipse (M_2) is rotated in the clockwise direction. The nonlinear rotation and the narrow ellipses observed in the diurnal and semidiurnal tidal ellipses show relatively unimportant rotation in the tidal flow and the importance of wave interference.

3.3 *Internal tides*

Harmonic analysis using the *T_Tide* Matlab package (Pawlowicz et al., 2002) was performed on the depth-averaging currents (barotropic), and the residual currents (baroclinic or internal tides) were obtained by subtracting the resulting tidal signal from the total currents at 5, 10 and 16 m depth. The baroclinic tidal currents were featured by flow with different directions at different depths. In order to get the first sight of internal tides (baroclinic) in the residual currents data, we performed the spectral analysis to the residual currents at different depths (5, 10 and 16 m) (Fig. 6). The existence of internal tides is confirmed if the spectral density shows the influence of tidal signal in the residual currents data. In addition, we also calculated the HKE to compare the energy between both barotropic tidal currents and residual currents (Fig. 7). The HKE calculated will determine whether the internal tides are negligible or not in this study.

Figure 6 presents the power spectral density plots of the barotropic currents and residual currents at certain depths. The results show the barotropic currents are predominated by 24 h and 12 h frequencies bands. The residual currents at 5, 10 and 16 m

Table 2. Ellipse parameters for diurnal (Q_1, O_1, P_1, K_1) and semidiurnal (N_2, M_2, K_2, S_2) harmonic constituents of depth-averaging (barotropic) currents

Year		Diurnal				Semidiurnal			
		Q_1	O_1	P_1	K_1	N_2	M_2	K_2	S_2
2013	Amp	0.017	0.120	0.042	0.131	0.015	0.071	0.016	0.007
	Pha	32.6	64.3	98.6	106.8	309.2	351.6	71.6	55.8
	Ecc	0.05	0.00	0.04	0.02	0.02	–0.02	–0.20	–0.12
2014	Amp	0.023	0.119	0.040	0.128	0.016	0.070	0.013	0.008
	Pha	55.4	59.3	110.3	107.0	327.8	349.9	63.4	67.8
	Ecc	0.01	0.00	0.09	–0.01	–0.01	–0.02	–0.19	–0.08
2015	Amp	0.021	0.115	0.042	0.127	0.013	0.070	0.013	0.011
	Pha	37.2	60.6	105.9	110.1	316.4	351.1	42.6	75.3
	Ecc	0.14	0.01	0.02	0.03	0.06	–0.02	–0.02	–0.11

Note: Amp represents amplitude in m/s, Pha phase in degree (°) and Ecc eccentricity of tidal ellipse.

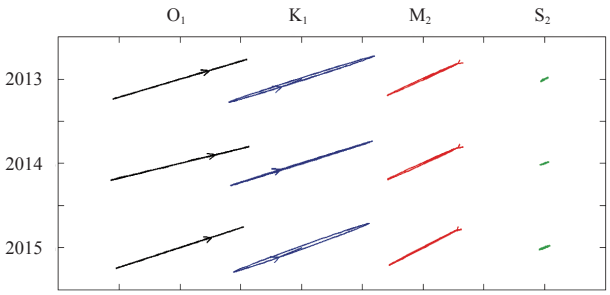

Fig. 5. Tidal ellipse of major tidal constituents of diurnal (O_1 and K_1) and semidiurnal (M_2 and S_2) barotropic currents in MJJA months of 2013, 2014 and 2015.

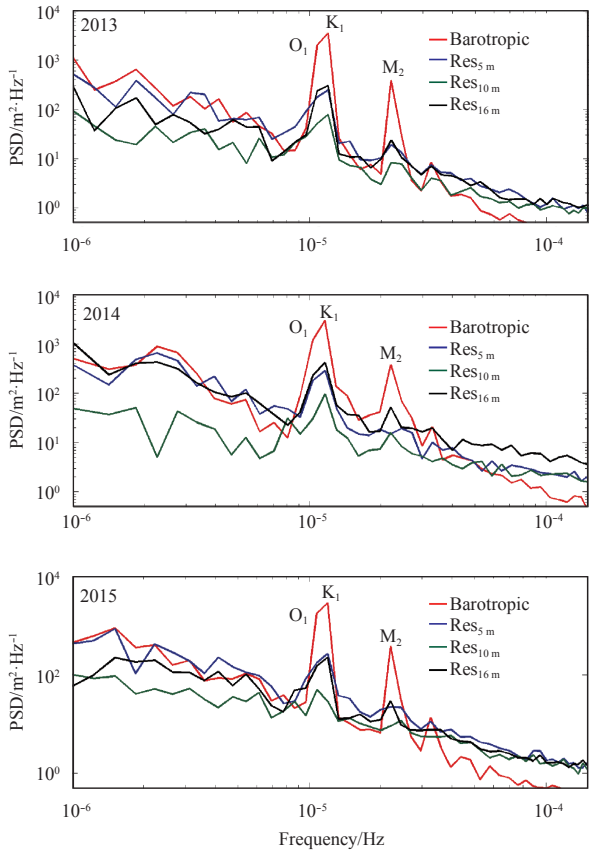

Fig. 6. Spectral density of barotropic tidal currents and residual currents at 5, 10 and 16 m in MJJA months of 2013, 2014 and 2015. The power spectral density is calculated based on 95% significance interval (not shown).

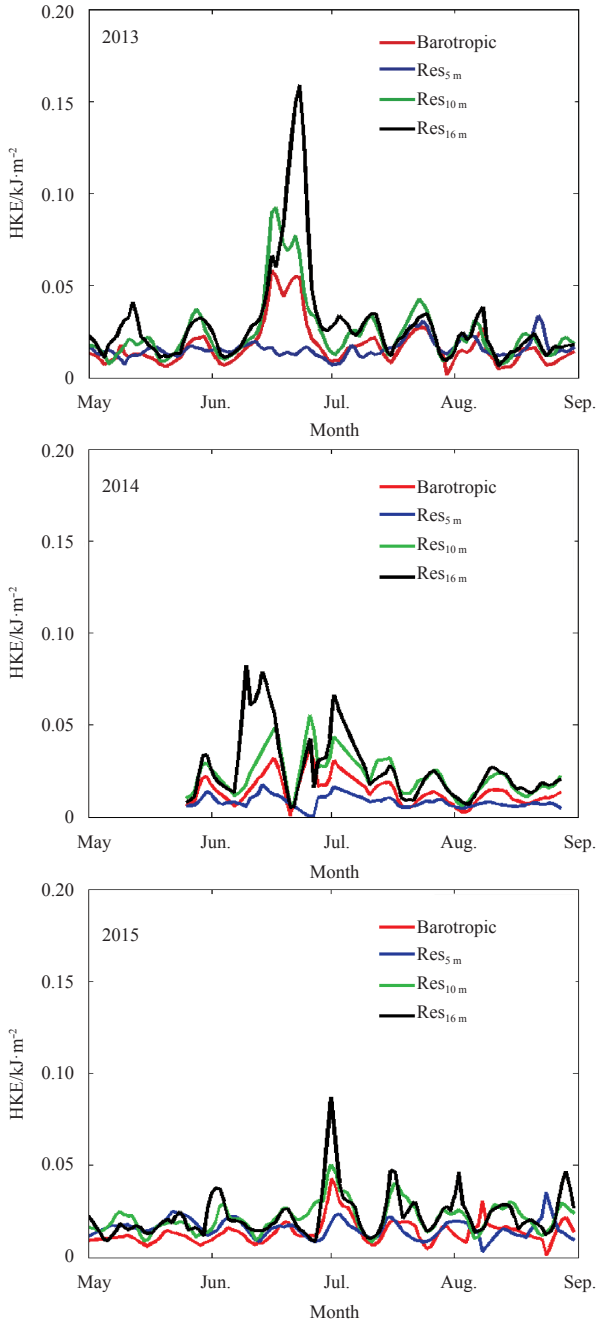

Fig. 7. Horizontal kinetic energy (HKE) of barotropic tidal currents and residual currents at 5 m, 10 m and 16 m depth in 2013 until 2015.

depth also showed a peak at 24 h frequency band and very small peak at 12 h frequency band indicating dominance effect of the diurnal tidal signal. The tidal signal in a detided series indicates the existence of internal tides in the currents data. In the near-surface (5 m) and near-bottom (16 m) of the water column, the diurnal variability of internal tides is greater than at 10 m depth (Fig. 6).

The HKE of residual currents presented in Fig. 7 shows that the existence of strong internal tides in the ECPM is intermittent. The energy of internal tides at 5 m is weak for all three years. The strongest energy of internal tides was observed at 10 m and 16 m depth during June and July (2013–2015). If compared with the temperatures series in Fig. 2, the strongest energy of internal tides at the near-bottom (16 m) is concomitant with the significant temperature drops in June and July (2013–2015). The fact that the internal tides energy is occasionally stronger than barotropic tidal currents; it shows that the internal tides in the ECPM area are something that cannot be ignored.

3.4 *Wavelet analysis*

The normalized wavelet power spectrums of each series (near-bottom temperature (16 m), near-bottom residual currents (16 m), barotropic currents and water level) are presented in Figs 8a, 9a and 10a. In all the three years, the diurnal normal-

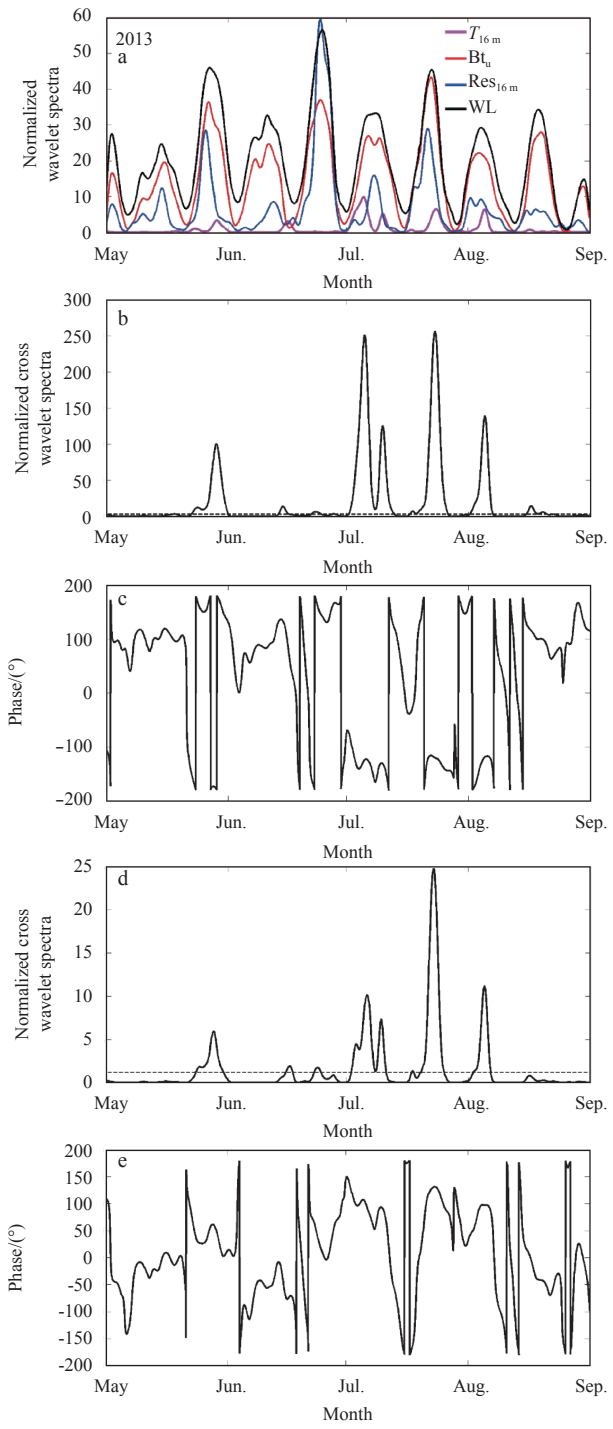

Fig. 8. Normalized wavelet power spectrum of near-bottom temperature, barotropic currents, near-bottom residual currents and water level (a), normalized cross wavelet spectrum between near-bottom temperature and barotropic currents (b) and phase angle (c), normalized cross wavelet spectrum between near-bottom temperature and near-bottom residual currents (d) and phase angle (e) for 2013. The spectra were normalized by the respective variances and significance levels so that the 95% confidence level equals 1 (marked by a dashed black line).

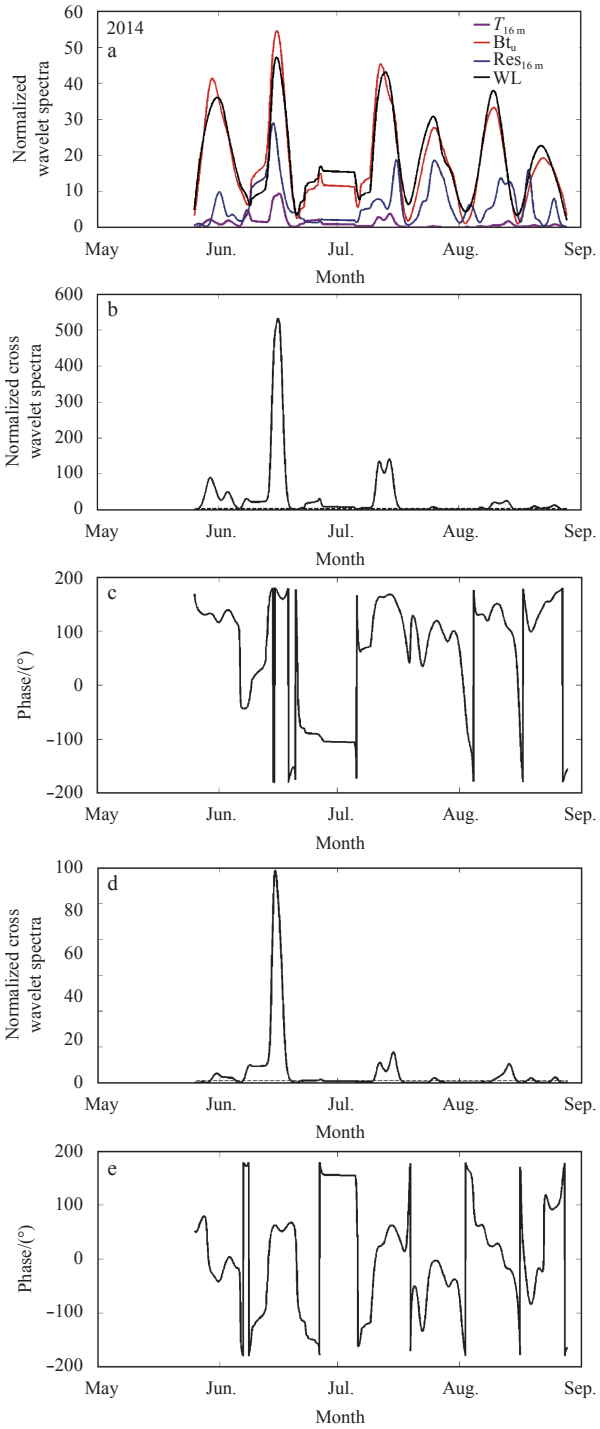

Fig. 9. Normalized wavelet power spectrum of near-bottom temperature, barotropic currents, near-bottom residual currents and water level (a), normalized cross wavelet spectrum between near-bottom temperature and barotropic currents (b) and phase angle (c), normalized cross wavelet spectrum between near-bottom temperature and near-bottom residual currents (d) and phase angle (e) for 2014. The spectra were normalized by the respective variances and significance levels so that the 95% confidence level equals 1 (marked by a dashed black line).

ized wavelet spectrum characters for barotropic currents and residual currents are related to water level fluctuation indicating the influence of tidal variability. Two significant peaks observed in every one month indicate the strong influence of spring-neap cycle in the diurnal currents. Strong wavelet spectra are probably related to spring tides phenomena while the weakest wavelet

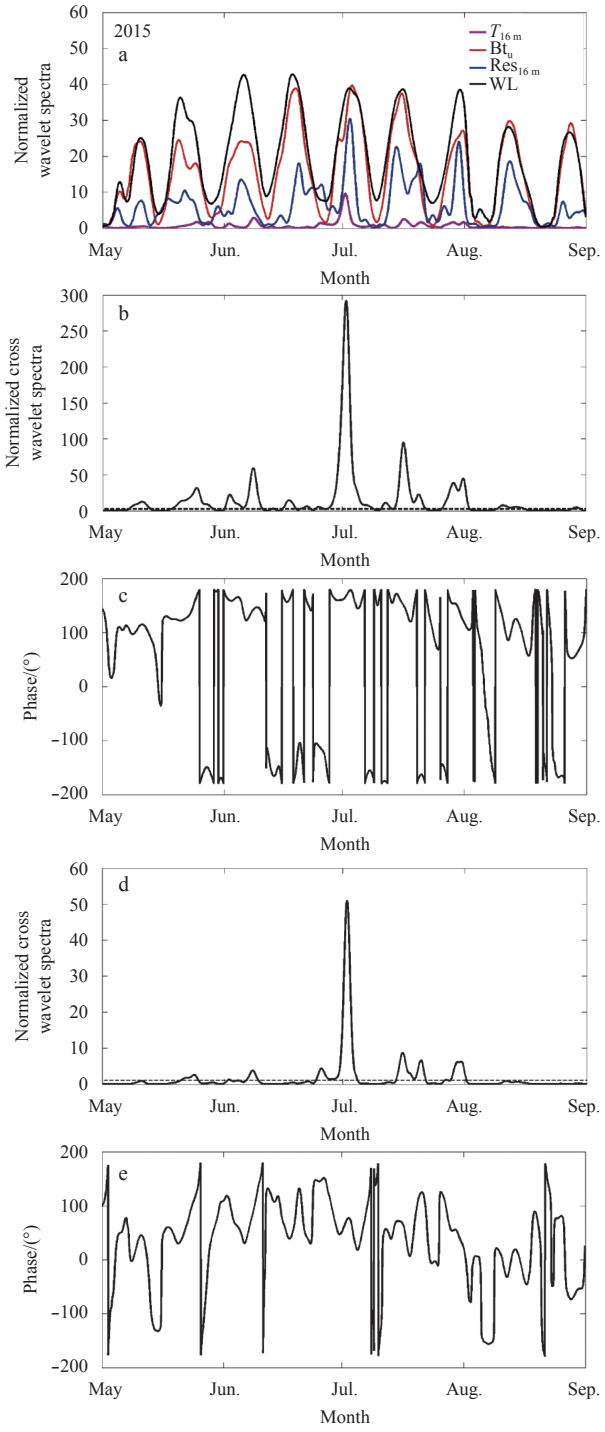

Fig. 10. Normalized wavelet power spectrum of near-bottom temperature, barotropic currents, near-bottom residual currents and water level (a), normalized cross wavelet spectrum between near-bottom temperature and barotropic currents (b) and phase angle (c), and normalized cross wavelet spectrum between near-bottom temperature and near-bottom residual currents (d) and phase angle (e) for 2015. The spectra were normalized by the respective variances and significance levels so that the 95% confidence level equals 1 (marked by a dashed black line).

spectra might be related to neap tides phenomena. Most of the time, the spectra of water level is almost similar to the barotropic currents except for in the end of June 2013 where the residual currents spectra surpassed the barotropic currents spectra (Fig. 8a). However, the near-bottom temperature spectra do not show any significant peak during the similar event. The biggest peak of near-bottom temperature was observed after the event (probably days after) (Fig. 8a). In 2014 and 2015, the highest peak of near-bottom temperatures spectra is concomitant with the high wavelet spectra of both barotropic and residual currents (Figs 9a and 10a).

The wavelet cross-correlation analysis was used to reveal the significant linear relationship and the relative phase between the response of the temperature and the exciting driver (in this case the barotropic currents and internal tides), presenting information on the phase relationship as a function of frequency. Zero-phase or minimum-phase differences can be considered as evidence of significant relationship (Ng and Chan, 2012b). The above spectral density plots had revealed the predominant importance of diurnal frequency band in the near-bottom temperatures and currents data (Figs 4 and 6). Thus, the normalized wavelet spectra of cross-wavelet transform between the near-bottom temperatures and currents are extracted and averaged over the diurnal period band; in this study are from 20 to 28 h (Figs 8, 9 and 10).

The correlation between the near-bottom temperature fluctuation and the dominant diurnal forcing mechanisms are presented in Figs 8, 9 and 10. In all the three years, the significant cross-correlation between the near-bottom temperature and both the currents (barotropic and residual) starting in June and the highest correlation (highest peak) was observed in July except for in 2014 where the highest peak was observed in the middle of June.

The wavelet cross-correlation revealed that during the first peak in June, near-bottom temperature fluctuations also showed some correlation in both cross-wavelet analyses with barotropic currents and residual currents. However, the phase angle shows minimum phase differences when correlated with residual currents than barotropic currents. Positive (0°–90°) mean phase angle indicates the in-phase relation between the near-bottom temperatures with both barotropic and internal tides in the ECPM. The mean phase angle of cross wavelet spectrum between near-bottom temperature and the diurnal barotropic tidal band for 2013, 2014 and 2015 are 32°, 85°and 56°, respectively (Figs 8c, 9c and 10c). The mean phase angle of cross wavelet spectrum between near-bottom temperature and the diurnal internal tide band for 2013, 2014 and 2015 are 11°, 5.6°and 38°, respectively (Figs 8e, 9e and 10e). These results indicate the strong relationship between residual currents and the near-bottom temperature when the significant sudden drops of near-bottom temperatures were observed (Fig. 2).

4 Discussion

The energy input through tidal forcing is the largest and most consistent mechanical forcing in most of the area of the coastal sea (Simpson and Sharples, 2012) including the ECPM shelf sea. This work presented the tidal currents characteristics (i.e., barotropic and internal tides) in the ECPM area based on high-frequency mooring data of currents and its relationship to the variability of near-bottom temperature. Most of the related previous studies were done in the whole region of SCS using the satellite altimetry data or model simulation outputs. In addition, this is the first time the internal tides were detected and studied in the ECPM area. The most significant outcome is their contribution to near-bottom temperature variability that has not been thoroughly addressed to our knowledge yet.

The most interesting part in the temperature series depicted

in Fig. 2 was the sudden decrease of near-bottom temperatures that mostly occurred in June and July. These sudden drops of temperatures were almost consistent for three consecutive years indicating permanent cooling event near the bottom of coastal ECPM during the southwest monsoon. The monthly average of cross-shore heat flux calculated from the near-bottom temperature and near-bottom cross-shore velocities also revealed the highest heat flux in June and July for all three years (Fig. 3). The highest heat fluxes indicate the intrusion of cooler water into the ECPM coastal seas are high in June and July (Fig. 3). The highest horizontal near-bottom heat flux observed in June might be related to the intrusion of cooler water similar to what was observed by Roseli et al. (2015). This cooler water was the mixed water that had its origin in the deep central basin of SCS (Dippner and Loick-Wilde, 2011). It probably was brought into the coastal of ECPM due to the upwelling event that mostly occurred in June when the southwest monsoon winds blow (Akhir et al., 2015; Dippner et al., 2007). However, the local mechanism that actually driven this upwelled water far into the ECPM coastal area remains unclear.

Other than monsoonal winds forcing, tides also are the predominant forcing in the coastal of ECPM. According to the spectral density and harmonic analysis results, the barotropic tidal currents are dominated by diurnal fluctuations of O_1 and K_1 tidal frequencies and semidiurnal M_2 tidal frequencies (Figs 5 and 7). This is consistent with previous studies (Daryabor et al., 2016; Taira et al., 1996; Yanagi et al., 1997; Zu et al., 2008), where the study area is characterized by mixed tides with dominant diurnal tides. Mixed tides in the mooring site exhibiting the strong diurnal inequality caused by the unequal heights in successive high or low water, or in both pairs of tides. As the mooring site located above the equator (5°N), it is possible to have strong diurnal inequality due to the changing angular distance of the moon above or below the equator.

Results of spectral density plots (Fig. 6) and HKE (Fig. 7) had confirmed the existence of internal tides in the ECPM coastal area. The spectral density plots show that the internal tides varied according to the diurnal tidal frequency. The existence of diurnal internal tides in the ECPM is probably due to the strong diurnal barotropic tidal currents (Figs 5 and 7) that interact with the steep slope at the central basin of SCS (~ 700 km away from the shoreline) (Fig. 1). This is because, the presence of spring-neap cycle in the diurnal internal tides associated with the prominent cycle in the barotropic currents (Figs 8, 9 and 10) suggests the internal tides are generated locally (Mihanović et al., 2009). The HKE results of barotropic tidal currents and residual currents (5, 10 and 16 m) showed that the existence of internal tides in the ECPM is intermittent. The peaks of internal tides energy that sporadically higher than the barotropic tidal currents indicated that the internal tides in the ECPM are not negligible. The strongest energy of internal tides was observed during the significant temperature drops in June and July and can be observed in all three years.

The presence of internal tides is always related to the stratified condition (Mihanović et al., 2009; Smith et al., 2016; Wang, 2012). Previous studies by using hydrographic data done in the ECPM area had revealed the seasonal variation of stratification in the area (Akhir et al., 2011, 2014; Akhir and Yong, 2011; Roseli et al., 2015; Roseli and Akhir, 2014; Yanagi et al., 2001), The stratification is the most stable in the southwest monsoon months with shallow thermocline layer (~20–30 m). In the monsoon transition month in October, the thermocline layer is deeper (~50 m) and almost none in the nearshore area.

While the surface water of ECPM receives high heat concentration in southwest monsoon and the stable stratification is well-developed, the warmer surface water and the near-bottom water are probably separated by a thermocline. In the ocean, when warm surface layer and cold deep layer separated by a thermocline, then motions on the interface or internal tides are possibly developed. Given the periodicity of main datasets used are during the southwest monsoon, it is well-known that during the southwest monsoon in June until early October, the sea surface temperatures in the southern region of SCS are warmer by approximately 2°C than in the other seasons due to greater heating from the sun (Akhir et al., 2011; Huang et al., 1997; Roseli et al., 2015; Saadon and Camerlengo, 1996). The attenuation of thermal flux within water column due to greater heat loss to the atmosphere enhanced the stratification during this season (Roseli et al., 2015; Yanagi et al., 2001). Thus, under this stratified condition, the internal tides were generated when the barotropic currents interact with the steep slope in the central basin of SCS. We loosely interpret that, during this time, the internal tides dissipate away to the shelf area and brought together the upwelled water into the ECPM coastal shelf sea. This is the reason why the short duration of cold pulse water was recorded at the near-bottom of ECPM in June and July when the stratification was the most stable. In order to evaluate the relative importance of internal tides and near-bottom temperature variability, we performed the cross-wavelet transform analysis to the barotropic tidal currents, residual currents (16 m) and near-bottom temperatures (16 m). The cross-wavelet analysis was performed in order to compare the two-time series by identifying their common power (Grinsted et al., 2004; Ng and Chan, 2012b). Considering the most dominant diurnal influence in the temperatures and currents from the spectral analysis results (Figs 4 and 6), the diurnal band was extracted from the cross-wavelet analysis (Figs 8, 9 and 10). The statistically significant cross-correlations between diurnal near-bottom temperature and diurnal barotropic currents (Figs 8b, 9b and 10b) and; between diurnal near-bottom temperature and diurnal residual currents (Figs 8d, 9d and 10d) occurred mostly in June and July for three consecutive southwest monsoon seasons.

Although both physical drivers of barotropic currents and internal tides showed high correlation with the near-bottom temperature variability in June and July, the phase angle relationship revealed other interesting feature during the cold pulse event. The minimum phase shift indicating a strong relationship between two series. Large phase shift was observed in the cross-wavelet spectra between the barotropic currents and the near-bottom temperature when the peak was observed (Figs 8c, 9c and 10c). Minimum phase shift was observed in the cross-wavelet spectra between the internal tides and the near-bottom temperature (Figs 8e, 9e and 10e). This observation remarked that, during the significant temperature drops in June and July, the relationship between the internal tides and the near-bottom temperature are strong compared to the relationship between the barotropic tidal currents and the near-bottom temperature. Although we cannot provide robust evidence of how much the water was transport by internal tides into the ECPM coastal shelf sea, the well-correlated and in-phase relationship between the internal tides and the near-bottom temperature is a positive sign that the internal tides probably propagate and brought together the cold water into the ECPM during the cooling event.

5 Conclusions

High-frequency series of water level and currents have been used to describe the variability of tidal forcing, and the relation-

ship with the near-bottom temperature variability in the coastal region of ECPM. The type of tides in the ECPM is the mixed tides with dominant diurnal tides. Water level and currents in the ECPM are predominantly influenced by diurnal (O_1 and K_1) and semidiurnal (M_2) tidal constituent with the highest amplitude was in the K_1 diurnal frequency.

To test the hypothesis about tidal dynamics forcing to the near-bottom temperature variability, we used cross-wavelet correlation analysis. Our results represent the well-tested linear relationship among barotropic currents fluctuation, internal tides, and near-bottom temperature fluctuations. A significant correlation between diurnal near-bottom temperature and diurnal internal tides was consistent with the sudden drops of temperature recorded in June and July for the three consecutive years. The relationship between the near-bottom temperatures and the physical drivers (barotropic currents and internal tides) showing that when the cooling period occurred, the internal tides were well-correlated with the near-bottom temperature fluctuation with minimum phase shift correlation.

This study revealed that even in a coastal area like ECPM, the internal tides at the diurnal frequency could possibly exist. Internal tides observed in this study was the first one detected in the ECPM region. Limited vertical and spatial datasets cannot determine the main mechanism that generates the internal tides in the ECPM coastal shelf sea. In the meantime, we loosely interpret that the internal tides developed due to the barotropic tidal currents that flow over the steep slope at the central basin of SCS under the stratified condition. Greater sea surface heating in MJJA months (warmer surface water) and the low-temperature water near the bottom enhanced the stratification within the water column. When the strong barotropic tidal currents interact with the sloping bathymetry under the stratified condition, the baroclinic energy is developed and dissipates over the shelf sea. When the upwelling occurred in June, the internal tides drove the pulse of cold water shoreward into the ECPM's near-bottom area.

Due to several unavoidable limitations in the study, further research can be done to improve to the knowledge contribution. The analysis that including the wind forcing and solar radiation as another physical driver that possibly contributes to the temperature variability in the ECPM could be done. In addition, the limited observed data on the middle shelf and shelf edge can be obtained by using numerical modeling or satellite altimetry data. This may help in explaining how much water the internal tide could transport into ECPM coastal shelf sea and the contribution of internal tides to the decreasing of temperature in June and July. At the same time, further research can be done to evaluate the relative importance of internal tides to monsoonal-induced upwelling that was observed in southwest monsoon season.

Acknowledgements

We gratefully acknowledge the crew members of Physical Oceanography & Geological Laboratory (POGL) of Institute of Oceanography and Environment (INOS), Universiti Malaysia Terengganu for their help in the AWAC profiler deployment and data collection.

References

Akhir M F M. 2012. Surface circulation and temperature distribution of southern South china sea from global ocean model (OCCAM). Sains Malaysiana, 41(6): 701–714

Akhir M F, Daryabor F, Husain M L, et al. 2015. Evidence of upwelling along Peninsular Malaysia during southwest monsoon. Open Journal of Marine Science, 5(3): 273–279, doi: 10.4236/ojms.2015.53022

Akhir M F, Sinha P C, Hussain M L. 2011. Seasonal variation of south china sea physical characteristics off the east coast of Peninsular Malaysia from 2002–2010 datasets. International Journal of Environmental Sciences, 2(2): 569–575

Akhir M F, Yong J C. 2011. Seasonal variation of water characteristics during inter-monsoon along the east coast of Johor. Journal of Sustainability Science and Management, 6(2): 206–214

Akhir M F M, Zakaria N Z, Tangang F. 2014. Intermonsoon variation of physical characteristics and current circulation along the east coast of Peninsular Malaysia. International Journal of Oceanography, 2014: 527587, doi: 10.1155/2014/527587

Bravo L, Ramos M, Sobarzo M, et al. 2013. Barotropic and baroclinic semidiurnal tidal currents in two contrasting coastal upwelling zones of chile. Journal of Geophysical Research: Oceans, 118(3): 1226–1238, doi: 10.1002/jgrc.20128

Chern C-S, Wang J. 1994. Influence of the seasonal thermocline on the intrusion of Kuroshio across the continental shelf northeast of Taiwan. Journal of Oceanography, 50(6): 691–711, doi: 10.1007/BF02270500

Chu P C, Edmons N L, Fan C W. 1999. Dynamical mechanisms for the south china sea seasonal circulation and thermohaline variabilities. Journal of Physical Oceanography, 29(11): 2971–2989, doi: 10.1175/1520-0485(1999)029<2971:DMFTSC>2.0.CO;2

Daryabor F, Ooi S H, Samah A A, et al. 2016. Tides and their dynamics over the sunda shelf of the southern South China Sea. PLoS One, 11(9): e0162170, doi: 10.1371/journal.pone.0162170

Dippner J W, Loick-Wilde N. 2011. A redefinition of water masses in the vietnamese upwelling area. Journal of Marine Systems, 84(1–2): 42–47, doi: 10.1016/j.jmarsys.2010.08.004

Dippner J W, Nguyen K V, Hein H, et al. 2007. Monsoon-Induced upwelling off the vietnamese coast. Ocean Dynamics, 57(1): 46–62, doi: 10.1007/s10236-006-0091-0

Grinsted A, Moore J C, Jevrejeva S. 2004. Application of the cross wavelet transform and wavelet coherence to geophysical time series. Nonlinear Processes in Geophysics, 11(5–6): 561–566

Huang Chiyue, Wu Sheufeng, Zhao Meixun, et al. 1997. Surface ocean and monsoon climate variability in the South China Sea since the last glaciation. Marine Micropaleontology, 32(1–2): 71–94

Kaplan D M, Largier J L, Navarrete S, et al. 2003. Large diurnal temperature fluctuations in the nearshore water column. Estuarine, Coastal and Shelf Science, 57(3): 385–398, doi: 10.1016/S0272-7714(02)00363-3

Ma B B, Lien R-C, Ko D S. 2013. The variability of internal tides in the northern South China Sea. Journal of Oceanography, 69(5): 619–630, doi: 10.1007/s10872-013-0198-0

Mihanović H, Orlić M, Pasarić Z. 2006. Diurnal internal tides detected in the adriatic. Annales Geophysicae, 24(11): 2773–2780, doi: 10.5194/angeo-24-2773-2006

Mihanović H, Orlić M, Pasarić Z. 2009. Diurnal thermocline oscillations driven by tidal flow around an island in the middle adriatic. Journal of Marine Systems, 78: S157–S168, doi: 10.1016/j.jmarsys.2009.01.021

Ng E K W, Chan J C L. 2012a. Interannual variations of tropical cyclone activity over the north Indian Ocean. International Journal of Climatology, 32(6): 819–830, doi: 10.1002/joc.2304

Ng E K W, Chan J C L. 2012b. Geophysical applications of partial wavelet coherence and multiple wavelet coherence. Journal of Atmospheric and Oceanic Technology, 29(12): 1845–1853, doi: 10.1175/JTECH-D-12-00056.1

Pawlowicz R, Beardsley B, Lentz S. 2002. Classical tidal harmonic analysis including error estimates in MATLAB using T_TIDE. Computers & Geosciences, 28(8): 929–937

Pidgeon E J, Winant C D. 2005. Diurnal variability in currents and temperature on the continental shelf between central and Southern California. Journal of Geophysical Research: Oceans, 110(C3): C03024, doi: 10.1029/2004JC002321

Robinson I S. 1983. Physical Oceanography of Coastal and Shelf Seas, Vol. 35. Netherlands: Elsevier, 469

Roseli N H, Akhir M F, Husain M L, et al. 2015. Water mass characteristics and stratification at the shallow Sunda shelf of southern

South China Sea. Open Journal of Marine Science, 5(4): 455–467, doi: 10.4236/ojms.2015.54036

Roseli N H, Akhir M F M. 2014. Variations of southern South China Sea characteristics near pahang. Sains Malaysiana, 43(9): 1389–1396

Saadon M N, Camerlengo A. 1996. Interannual and Seasonal Variability of the Mixed Layer Depth of the South China Sea. In: National Conference and Climate Change. Selangor, Malaysia: Universiti Putra Malaysia, 141-151

Simpson J H, Sharples J. 2012. Introduction to the Physical and Biological Oceanography of Shelf Seas. New York, Cambridge University Press, 90

Smith K A, Rocheleau G, Merrifield M A, et al. 2016. Temperature variability caused by internal tides in the coral reef ecosystem of Hanauma Bay, Hawai'I. Continental Shelf Research, 116: 1–12, doi: 10.1016/j.csr.2016.01.004

Subeesh M P, Unnikrishnan A S. 2016. Observed internal tides and near-inertial waves on the continental shelf and slope off jaigarh, central west coast of India. Journal of Marine Systems, 157: 1–19, doi: 10.1016/j.jmarsys.2015.12.005

Taira K, Nasir M N B, Kitagawa S, et al. 1996. Observation of temperature and velocity in the coastal water off Kuala Terengganu, Malaysia. Journal of Oceanography, 52(2): 251–257, doi: 10.1007/BF02235673

Tangang F T, Xia Changsui, Qiao Fangli, et al. 2011. Seasonal circulations in the malay peninsula eastern continental shelf from a wave-tide-circulation coupled model. Ocean Dynamics, 61(9): 1317–1328, doi: 10.1007/s10236-011-0432-5

Torgrimson G M, Hickey B M. 1979. Barotropic and baroclinic tides over the continental slope and shelf off oregon. Journal of Physical Oceanography, 9(5): 945–961, doi: 10.1175/1520-0485(1979)009<0945:BABTOT>2.0.CO;2

Wang Dongping. 2012. Diurnal modulation of semidiurnal internal tides in luzon Strait. Ocean Modelling, 59–60: 1–10, doi: 10.1016/j.ocemod.2012.09.005

Wu Lidan, Miao Chunbao, Zhao Wei. 2013. Patterns of K1 and M2 internal tides and their seasonal variations in the northern South China Sea. Journal of Oceanography, 69(4): 481–494, doi: 10.1007/s10872-013-0183-7

Wyrtki K. 1961. Physical Oceanography of the Southeast Asian Waters, Vol. 2. La Jolla, California: The University of California, Scripps Institution of Oceanography, 195

Yanagi T, Sachoemar S I, Takao T, et al. 2001. Seasonal variation of stratification in the Gulf of Thailand. Journal of Oceanography, 57(4): 461–470, doi: 10.1023/A:1021237721368

Yanagi T, Takao T, Morimoto A. 1997. Co-tidal and Co-range charts in the South China Sea derived from satellite altimetry data. Marine Engineers Review, 35(3): 85–93

Zhang W G, Duda T F, Udovydchenkov I A. 2014. Modeling and analysis of internal-tide generation and beamlike onshore propagation in the vicinity of shelfbreak canyons. Journal of Physical Oceanography, 44(3): 834–849, doi: 10.1175/JPO-D-13-0179.1

Zu Tingting, Gan Jianping, Erofeeva S Y. 2008. Numerical study of the tide and tidal dynamics in the South China Sea. Deep Sea Research Part I: Oceanographic Research Papers, 55(2): 137–154, doi: 10.1016/j.dsr.2007.10.007